IEEE Access
Multidisciplinary ⋮ Rapid Review ⋮ Open Access Journal

Received 4 May 2023, accepted 21 June 2023, date of publication 28 June 2023, date of current version 11 July 2023.

Digital Object Identifier 10.1109/ACCESS.2023.3290904

RESEARCH ARTICLE

Effects of Patient Recumbency Position on Neonatal Chest EIT

N. SEIFNARAGHI[1], S. DE GELIDI[1], I. FRERICHS[2], M. KALLIO[3,4], MD. E. SORANTIN[5], A. DEMOSTHENOUS[6], (Fellow, IEEE), AND R. H. BAYFORD[1], (Life Senior Member, IEEE)

[1]Department of Natural Sciences, Middlesex University London, NW4 4BT London, U.K.
[2]Department of Anesthesiology and Intensive Care Medicine, University Medical Centre Schleswig-Holstein, 24105 Kiel, Germany
[3]PEDEGO Research Unit, Medical Research Center, University of Oulu, 90570 Oulu, Finland
[4]Department of Children and Adolescents, Oulu University Hospital, 90220 Oulu, Finland
[5]Department of Radiology, Medical University of Graz, 8036 Graz, Austria
[6]Department of Electronic and Electrical Engineering, University College London, WC1E 6BT London, U.K.

Corresponding author: N. Seifnaraghi (n.seifnaraghi@mdx.ac.uk)

This work was supported in part by the Continuous Regional Analysis Device for neonate Lung (CRADL) Project (http://cradlproject.org) funded by the European Union's Horizon 2020 Research and Innovation Program (2014–2018) under Grant 668259, and in part by the Engineering and Physical Sciences Research Council (EPSRC) under Grant EP/T001259.

ABSTRACT This paper investigates the overlooked effects of the patient recumbency positions on one of the key clinically used parameters in chest electrical impedance tomography (EIT) monitoring – the silent spaces. This parameter could impact medical decisions and interventions by indicating how well each lung is being ventilated. Yet it is largely dependent on assumptions of prior model at the reconstruction stage and the closely linked region of interest (ROI) during the final calculations. The potential effect of switching recumbency modes on silent spaces as a results of internal organ movements and consequently changes in initial assumptions, has been studied. The displacement and deformations caused by posture changes from supine to lateral recumbent were evaluated via simulations considering the simultaneous gravity-dependent movement and/or deformations of heart, mediastinum, lungs and the diaphragm. The reliability of simulations was verified against reference radiography images of an 18-month-old infant in supine and decubitus lateral positions. Inspecting a set of 10 patients from age range of 1 to 2 years old revealed improvements of up to 30% in the silent space parameters when applying posture consistent amendments as opposed to fixed model/ROI to each individual. To minimize the influence of image reconstruction technique on the results two different EIT reconstruction algorithms were implemented. The outcome emphasized the importance of including recumbency situation during chest EIT monitoring within the considered age range.

INDEX TERMS Electrical impedance tomography, internal organ displacements, lung deformation neonatal chest EIT, recumbency position, thorax modeling.

I. INTRODUCTION

Electrical impedance tomography (EIT) was developed in the early 1980s [1]. It is capable of providing an electric conductivity image of a domain using electrodes attached to the boundary surface of that domain [2]. Small alternating currents are injected through specific electrode pairs and the resulting potential differences on the remaining electrodes are measured and used to reconstruct a conductivity image. Despite the low spatial resolution of EIT relative to other imaging techniques like computed tomography (CT) and magnetic resonance imaging (MRI), the virtues of being non-invasive and providing high temporal resolution, which enables dynamic functional imaging, have made EIT desirable in the clinical field. EIT has been used in a number of medical applications including brain imaging [3], [4], [5], detection of breast cancer [6], [7], hepatic tumors [8] and respiratory system monitoring [9], [10], [11]. The latter exploits the significant change in the intrathoracic electrical conductivity as lungs' air content varies during respiration which makes EIT suitable for continuous bedside respiratory monitoring. EIT has been successfully used to image regional

The associate editor coordinating the review of this manuscript and approving it for publication was Eduardo Rosa-Molinar.

changes in pulmonary ventilation and perfusion in real time.

With regards to monitoring neonatal and small children, lung EIT is desirable as it neither carries hazardous radiation effects like a CT scan nor the complications of MRI such as being time costly and often the requisite of sedation. The other advantage is the capability of EIT providing dynamic images. An example could be the situation where a clinician is interested to evaluate the impact of a clinical intervention performed on the patient earlier.

Studies in newborn infants and children have demonstrated quantitatively identifiable changes in regional lung aeration and ventilation following alterations to respiratory support and interventions such as a recruitment maneuver, surfactant administration or nursing procedures [12], [13].

One of the main challenges in EIT is solving the inverse problem to reconstruct the conductivity image since the solution is not unique as many different conductivity distributions may lead to the same measured electrode potential differences. In addition, direct inversion of system matrix which relates boundary measurements to input injections would be too sensitive to noise causing ill-posedness. Many attempts have been made to improve the quality of reconstructions, for example, by implementing various inverse problem conditioning and solutions [14], [15], [16], [17], [18], [19].

However, there have been very few attempts to improve the inverse solution by adapting the model to the situation of an individual patient. This should not be confused with patient specific modelling as it has already been shown that, improving the model not only impacts the reconstructed images [20] but also has a direct impact on clinical parameters [21]. Here, the focus is the effect of patient recumbency even though when a rough prior model estimate was used, the effect should be considered during clinical parameter calculations.

Typically, the prior models that regions of interest (ROI) are defined upon, are created based on averaged contours retrieved from CT scans. This is exacerbated when the patient is in the early years of life, as this patient group do not routinely undergo CT scanning due to exposure to X-rays. Consequently, there is limited data available corresponding to this age group. Moreover, the relatively small patient sizes combined with low spatial resolution demand implications of all possible improvements in modelling and reconstructions.

In this work, it has been attempted to indicate the internal aspects of the assumed model amid recumbency position. Despite the possibility of estimating the exterior deformation of the chest at the nipple line level of the patient where the EIT electrode belt is placed, using sensors [22] the internal changes of lung contour cross-sections cannot be estimated externally as the patient switch to various recumbency positions.

Only few studies have investigated the displacement of internal organs in-vivo; [23] in awake mode and the rest are mainly focusing on surgical operations in lateral posture and anesthesia [24], [25]. To our knowledge, no attempt has been made to address this issue in infants and studying its effects on lung EIT.

In this paper, we have investigated the impact of possible displacement of heart, mediastinum and diaphragm on deforming lungs and the corresponding outcome on the extracted clinical EIT parameter namely, silent spaces [26]. This parameter shows the percentage of each lung area that is not being ventilated during breathing, it represents the silent lung areas that do not exhibit ventilation-related impedance variation typically due to alveolar overdistension or collapse. It is one of the main clinical parameters for the assessment of clinical interventions [27].

The extent of thoracic movements as a result of recumbency change could be evaluated using simulations, should the reliable mechanical properties of the involved organs within the considered age range be available. However, the available data mainly include adults. In addition, the lungs as two of the major components in the thoracic region show different mechanical characteristic at various inflation rates, for instance they could enter to hyper-elastic regime in high air volume rate where the pressure-volume relation is not linear anymore [28]. Hence the mechanical properties are estimated starting from available adults and adopted to younger ages using anatomical development information combined with 18 months baby radiographs as a reference.

Understanding the movement of internal organs in a quantitative manner would help designing models and ROIs capable of adapting to real life patient recumbency mode and therefore, more accurate EIT parameter.

The rest of the paper is organized as follows. Section II describes the proposed method for estimating the changes occurring during recumbency position change from supine to either of two lateral positions, and how the simulated results compare to practice. In Section III the effect of consideration of adapting model to body position is examined via the calculation of silent spaces as a quantitative measure. Discussion of the results and concluding remarks are detailed in Section IV and V respectively.

II. METHOD

To evaluate the effect of recumbencies on the calculated silent spaces, images and subsequently the silent spaces were computed using the EIT signal from a known lateral position assuming two different scenarios; the situation when the considered prior and hence ROI were consistent with the patient's actual recumbency position against the situation in which the prior was set to the default mode corresponding to patient being at supine mode. This approach was chosen to limit the involved variables and help to focus on the internal changes within the same individual in various recumbency modes.

Ideally, both the exterior shape where EIT signal is recorded and an estimate of the cross-sectional organ contours at the same transversal plane are available, however, in practice such information specifically regarding the internal contours is often missing.

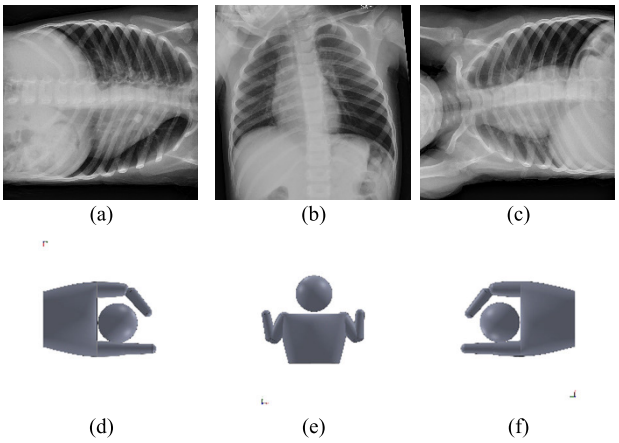

FIGURE 1. Chest X-rays showing internal organ configuration change of the same patient during change in recumbency position; (a) left lateral, (b) supine and (c) right lateral, (d)-(f) the corresponding schematics.

Thus, to mimic such situations, models needed to be designed capable of describing the contour variations as a function of recumbency state. These models were initially created based on CT scans at supine whereas lateral models were reproduced via simulations considering the gravity forces and the mechanical properties of the involved organs.

As the mechanical properties of the desired tissues were not available in the literature for the considered age range and the in-vivo situation, these values needed to be adopted from their adult range counterparts. To do this, a reference case study was used. there are not many situations, where the same patient undergoes CT scan for few times having a different recumbency position during each. The same is valid even for methods with no hazardous radiation like MRI. This issue aggravates further when considering the infants and neonatal age group.

There are, however, occasions when chest X-ray radiography are taken in decubitus lateral in addition to typical supine/standing positions. This technique allows to evade the negative impact caused by superimpositions of organs via exploiting the movement of heart and mediastinum consequently avoiding potential inhaled foreign bodies or irregularities being masked on the final projected image on the radiology film.

The reference images were taken from [29] and shown here in Fig. 1 at three different positions belonging to a 1.5 years old boy who was admitted to hospital because he inhaled a foreign body while playing in the yard.

The reference image was used to verify whether the results of the chosen mechanical properties while conducting the simulations could match the internal movements occurring in practice. Considering the 2D nature of reference X-ray images these simulations were limited to the same dimensions.

Four major potential factors regarding anatomical organ distribution in the thoracic cavity in the course of recumbency changes were taken into account. The deformation of rib cage, the displacement of the heart and mediastinum towards the engaged side under the effect of gravity, deformation/compression of the dependent lung due to its own weight and pressure applied by heart and mediastinum and lastly the change in diaphragm shape amid the pressure from abdominal cavity.

As the heart resembles a cone the distribution of the weight is not uniform hence causing a torque and thus rotating slightly as a result. The rotation of heart in the axial plane around its centroid creates less wide shadow on the radiography film during lateral left and conversely widest within lateral right where the width is measured as linear distance between the apex of the heart to the furthest point on the opposite side.

The abdominal sack is bounded peripherally to abdomen muscles and caudally to pelvic muscles, however, in cranial direction is limited to the thin diaphragm which mostly bears the weight of the heart and lungs. Therefore, during the right lateral recumbency they tend to shift to the right side of the patient, intensifying the pressure of the liver below the right lung towards cranial direction. The reverse is true when in left lateral as the pressure caused by liver eases and diaphragm dome shift towards the left side. The shape changes of the diaphragm from abdominal contents also lead to an additional rotation of the heart in the coronal plane.

Regarding the outer deformation, earlier studies on adults suggest that compared to the standing position the supine and prone positions expand in lateral directions and compressed in ventral-dorsal direction whereas the opposite is true in lateral recumbency [30]. To evaluate the extent of such behavior and verify if this deformation would be still relevant in infants, the decubitus lateral reference images were superimposed on the frontal supine image. This would reveal if the maximum side to side distance was affected noticeably. It should be noted maximum is considered that the projection of the 3D chest on the film was available hence no information could be retrieved regarding ventral-dorsal direction.

A. PREPARATION OF REFERENCE IMAGES

To perform a fair comparison among images and further use for simulation verification purposes, the reference images had to be adjusted according to two possibilities.

1) SCALING

Unlike CT scans and MR images, X-ray images do not contain scaling information. Therefore, the reference images should be homogenized in scale both among the reference images themselves and further to a reasonable dimension corresponding to a real human subject of similar anatomical features. Therefore, the image in supine position was scaled exploiting the CT scan of a male patient of 1.5 years old in a manner that the corresponding width of the image matched the coronal 2D projection of the 3D CT-scan based model. This image was then used for homogenizing the scale of the

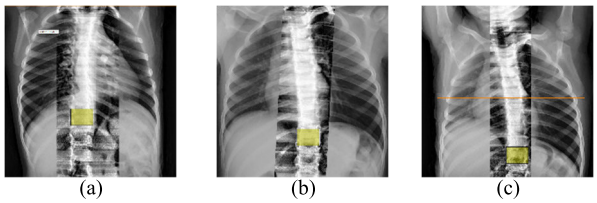

FIGURE 2. Scaling and positioning of internal tissues based on a chosen pixel covering the vertebrae at the intercostal of 11th and 12th ribs.

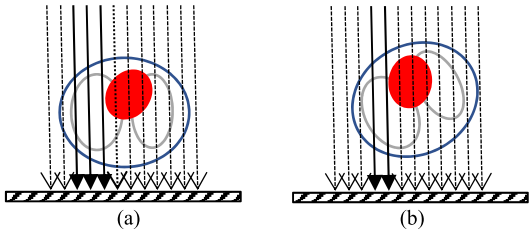

FIGURE 3. Schematic drawing of thorax cross-section and passing X-rays in frontal chest radiography, (a) correct alignment, (b) rotated.

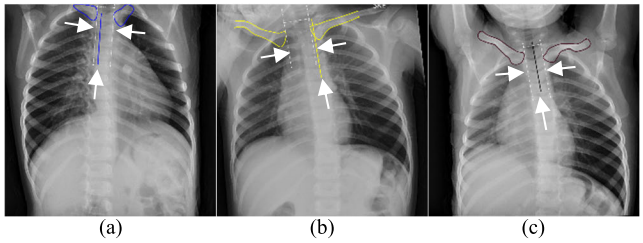

FIGURE 4. Spinous process line versus clavicle head bones at the sternum side, (a) left lateral, (b) supine and (c) right lateral.

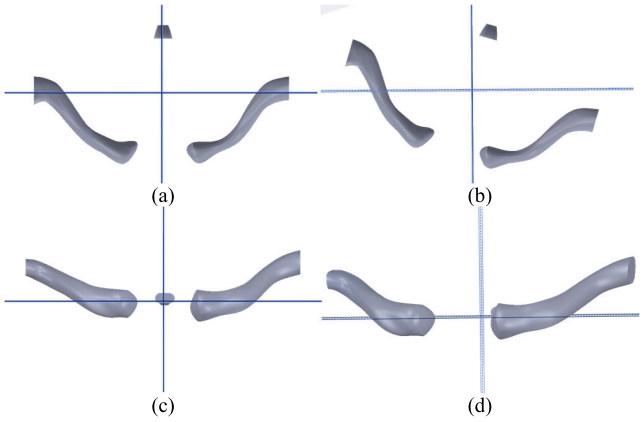

FIGURE 5. Spinous process and clavicle bones, (a) top view aligned, (b) top view rotated, (c) frontal view aligned, (d) frontal view rotated.

remaining lateral images using the 11^{th} and 12^{th} vertebrae as a criterion as they have very limited rotational movement or deformation during recumbency position changes and also position/angle of the arms, neck and head.

A large rectangular pixel was created to cover the 11^{th} and 12^{th} vertebrae of the spine when in supine with its corners located at the centers of rib facets. For the scaled supine image this was measured to be 21.36 mm width and 15.89 mm in height. The same rectangle was detected in lateral films and scaled to match the size and the position of the original pixel to uniform the scaling and facilitate the superimpositions. The procedure is highlighted in semi-transparent yellow in Fig. 2.

The side-to-side distance at the level of the 6^{th}-7^{th} intercostal space at the spine during supine position was measured 136.14 mm compared to the left lateral and right lateral positions at 131.07 mm and 134.68 mm respectively. This is in line with earlier studies for adults, indicating there is a deformation in thoracic cross-section but not affecting the transversal rib cage [25]. Moreover, within each lateral image one can notice the change in shape of the ribs 5-10 as they have come closer and less curved under pressure relative to the opposite side which is not bearing any load.

2) ADJUSTING ROTATION

It is not uncommon to have rotations in supine anterior-posterior (AP) chest radiography. This can be checked by comparing the lateral distance of each clavicle at the sternum side to the vertical line connecting the spinal process.

This rotation impacts the appearance of lung sizes and position of the heart on the film and hence should be adjusted. Fig. 3 illustrates a schematic example of such impact whereas the number of exposed rays passing through right lung in the correctly aligned patient reduces amid the misalignment creating a narrower shadow corresponding to this lung.

In frontal chest radiography the patient is considered to be correctly aligned when the clavicle heads at sternoclavicular joints on the film appear equally distant from the vertical line passing through spinous process of the vertebrae. Any spinous deviation from the mid-line towards clavicles indicates possible rotation of patient in the corresponding side from the aligned position.

These lines are highlighted and marked with arrows in Fig. 4 for supine and left and right lateral decubitus.

Prior to further analysis, this artefact should be checked and compensated for. To do that, the 3D model applied in the previous section for scaling was used to simulate the status of the available frontal radiography by designing the clavicle bones and rotating until the projected image matched the reference image. The top row panels in Fig. 5 show the top view of the correctly aligned mode in Fig. 5(a) and the similar rotation to the reference image in Fig. 5(b) where the bottom row illustrate the corresponding situation from frontal view as would be seen on the emitted X-rays. It is evident when the patient is rotated around the longitudinal axis towards the right side the spinous process is projected closer to the head of the left clavicular bone until completely masked. The simulation revealed within the model dimensions, a rotation of approximately 16.5 degrees could lead to such a situation.

To compensate for this effect the 3D models of clavicle bones, lungs and heart were rotated at opposite direction for 16 degrees and projected on a coronal 2D plane to mimic the projection during radiography. The correctly aligned

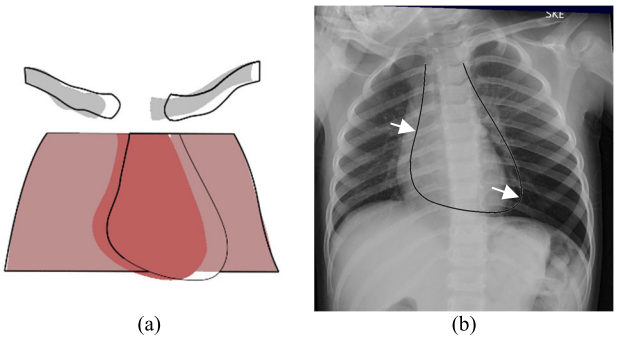

(a) (b)

FIGURE 6. Alignment compensation for lungs, clavicles and the heart appearance on the radiology film before rotation adjustment and after reverting back the rotation to the aligned mode outlined with solid black lines, (a) designed model, (b) superimposed on the film.

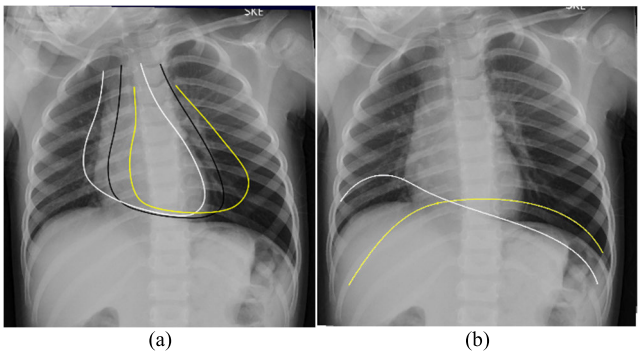

(a) (b)

FIGURE 7. The position of heart and diaphragm during, (a) right lateral, (b) left lateral plotted with white and yellow solid lines respectively.

positions are drawn with a solid black line over the rotated version in Fig. 6(a) and over the supine reference X-ray image in Fig. 6(b).

B. EVALUATION OF MOVEMENTS

The comparison of these projection modes showed an 8 mm displacement of the projected heart towards the right side when rotated. In addition, there was also a shrinkage of 6 % in the size of the corresponding projected area relative to the aligned mode. The image shown in Fig. 7(a) demonstrates the outline of the heart in black when supine and rotational impacts are compensated for whereas the contours in yellow and white indicate the same contours in left and right laterals respectively.

The heart apex transitional traveled distance was measured at 26.67 mm in the course of change from one lateral position to the other. This emphasizes the potentially higher significance of internal configuration change relative to exterior rib cage deformation amid the recumbency position. However, this does not imply that there is no deformation in exterior contour of thorax cross-section as there are other contributing factors but rather it suggests that the change in maximum transversal dimension within the rib cage is negligible at this age range. It appears like the heavier base side of the heart moves towards the dependent lateral side causing a rotation in axial plane. Consequently, a wider area becomes exposed to the beam.

The other aspect of the heart movement is its rotation in coronal plane. Here, the underlying basis is the movement of diaphragm which in turn is related to pressure distribution change in the cranial direction. As the individual goes through various recumbency positions the abdominal contents start to move accordingly. These tissues are bounded laterally and in anterior posterior sides by abdominal muscles and caudally by pelvic muscles. Due to the lesser resistance provided by the relatively thin diaphragm muscle and elastic lungs, the abdominal organs could be pushed cranial according to recumbency position. This can be seen by the elevation of the right dome of diaphragm during right lateral where the liver tissue is nestling and the base of the heart. On the left lateral though the liver pressure will shift towards the medial region while the stomach as a hollow container not able to pressurize the left dome upwards relative to the liver resulting in a flatter positioning of the heart in caudal side. The movement of diaphragm in the case study used here conforms with an earlier study where the diaphragm movement during various recumbency positions was reported in adults [31]. Fig. 7(b) plots the superimposed diaphragm lines according to positions.

C. SIMULATION OF MOVEMENTS AND VERIFICATION

Considering the small strain displacements relative to the geometry domain dimensions and the fact that the heart as the main rigid domain is initially in contact with the elastic lung domain in addition to application of small incremental load steps during simulations for both better convergence and mimicking the physiological transition from supine to lateral, the governing equations can be assumed to be linear.

$$\nabla \cdot \boldsymbol{\sigma} + \mathbf{F} = 0 \tag{1}$$

$$\boldsymbol{\varepsilon} = {}^{1}\!/_{2}(\nabla \mathbf{u} + (\nabla \mathbf{u})^{\mathrm{T}}) \tag{2}$$

$$\boldsymbol{\sigma} = \mathbf{C} : \boldsymbol{\varepsilon} \tag{3}$$

where $\boldsymbol{\sigma}$ is the material stress tensor and $\mathbf{F}$ is the external force per unit volume. The displacement tensor $\mathbf{u}$ is assumed to move with no acceleration hence the right-hand side of (1) turns to zero. $\boldsymbol{\varepsilon}$ stands for the infinitesimal strain tensor simplified amid the assumption of linear strain displacements causing the second order spatial gradients of $\mathbf{u}$ to be neglected in (2). $\mathbf{C}$ represents the 4^{th} order stiffness matrix and as a function of bulk and shear moduli valid for elastic materials according to Hooke's law. The symbol : indicates the tensor inner product as $\mathbf{C} : \boldsymbol{\varepsilon} = \mathrm{C}_{ij}\varepsilon_{ij}$.

Two scenarios of changing recumbency position from supine to either right or left laterals were examined.

The contribution of abdomen cavity and mediastinum were introduced as boundary loads. The abdominal contents impact was reflected as a single organ representing all of the involved organs since they are similar in density and stiffness. Furthermore, these are bound by a hermetic airtight adhesive contact among its contents via parietal and visceral

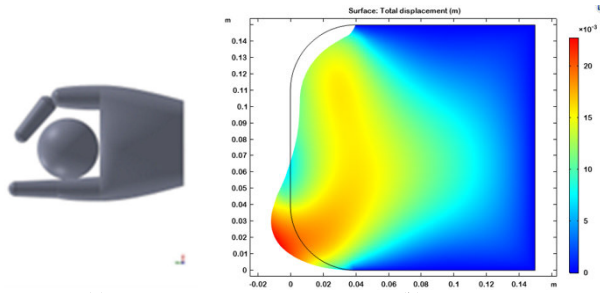

FIGURE 8. The simulated diaphragm movement during right lateral, (a) schematic position of patient, (b) total displacements.

peritoneum lining entire abdomen and intra-abdominal contents respectively [32]. Hence, the organs in proximity to each other move together making the cavity uniform from the mechanical point of view [33] with anchoring ligaments preventing large movements. These organs were all presumed to have the same material features similar to the liver [30] representing the dominant organ in the considered domain. The diaphragm was assumed to be more flexible within the medial regions and stiffer near the edges where it connects to bony structure of the ribs.

Using the 3D CT scan-based model a simplified rectangular shape with comparable dimensions was created. The edges were rounded at the cranial side to be able to deform freely since the total weight of the abdominal contents are larger than the thoracic cavity making the pressure caused from caudal side dominant. Moreover, fixed boundaries were prescribed at the right and left sides where the diaphragm is connected to the rib cage and large intestines being anchored to the abdominal walls. The situation of right lateral mode is plotted in Fig. 8 where Fig. 8(a) shows the schematic recumbency and Fig. 8(b) depicts the total displacement of abdominal content.

The pressure of the organs on the non-dependent side due to gravity force increases as the depth gets larger towards the dependent side causing organs to press and force the diaphragm to cranial direction more in the deeper sections. The results are in line with both the previous studies in [34] where it was reported the diaphragm shape would follow a mostly linear pattern and the earlier observations of superimposition shown in Fig. 7(b).

The combined rib cage and supporting platform was modeled as a continuous high stiffness surface boundary via springs with large spring constants at the normal direction to the surface. The function describing the spring constant was defined so that the values assigned were higher at the parts the patient's rib cage had minimal distance from the supporting platform (bed).

The studies emphasizing the lungs' mechanical property as hyper-elastic material [35] would be irrelevant in this work as within the expected compression/expansion range, the relation between stress and strain in macroscale could be assumed as linear. Hence, the lungs were treated as a linear elastic material [36].

TABLE 1. Mechanical property values of biological tissues.

Modeled Tissue	Density [kg/m^3]	Bulk Modulus [N/m^2]	Shear Modulus [N/m^2]	Stiffness [N/m]
Lungs	300	735	490	-
Heart	1060	inf	inf	-
Ribs	1400	-	-	5e5

Considering the stiffness of the lungs as a porous sponge like material relative to the muscular structure of the heart, the heart was assumed as a rigid material meaning it would not deform amid the pressures applied from lung weights. The mediastinum was prescribed as a load equal to the heart with exponential decrement towards cranial side to include the effect of surrounding membranes connected to posterior side of sternum.

The independent upper lung weight was neglected as the inter-pleural pressure would not allow the detachment of the upper lung from the neighboring chest wall. However, as the mediastinum and heart move to the dependent side, upper lung expands to fill the created space.

The mechanical property values listed in Table. 1 were applied in the conducted simulations [37], [38]. For simplicity the lungs were assumed to be at functional residual capacity (FRC) volumes where the expiration had ended and inspiration not begun yet hence there is no air exchange and a content intrapleural pressure at -5 cmH_2O [39]. Applying the relation between age, weight, height, gender and the heart weight reported in [40] and [41], the modelled patient's heart was assumed to be at 0.07 kg.

The meshing of the finite element method (FEM) was performed in a fine manner specifically at the boundaries of the heart and lung domains to enable appropriate handling of the concave contacts.

The simulations confirmed the significant displacement of heart and diaphragm along with considerable compression of lung amid the change in recumbency. Fig. 9 and Fig. 10 illustrate the occurring transitions at 10, 50, and 100% of the applied loads for right lateral and left lateral respectively.

The black lines indicate the original position of lungs and heart prior to lateral position when the patient was supine. The superimposition of the results on the X-ray reference images plotted in Fig. 9(d) in right lateral posture and Fig. 10(d) during left lateral showed the changes in anatomical configurations during recumbency change were consistent with the simulated results.

D. IMPACT ON SILENT SPACES

The silent spaces parameter indicates the percentage of lung volume with little or no ventilation. To evaluate the recumbency impact, a common EIT signal was simulated in lateral mode with two reconstruction scenarios. First when the applied model (hence, ROI) was kept at default supine

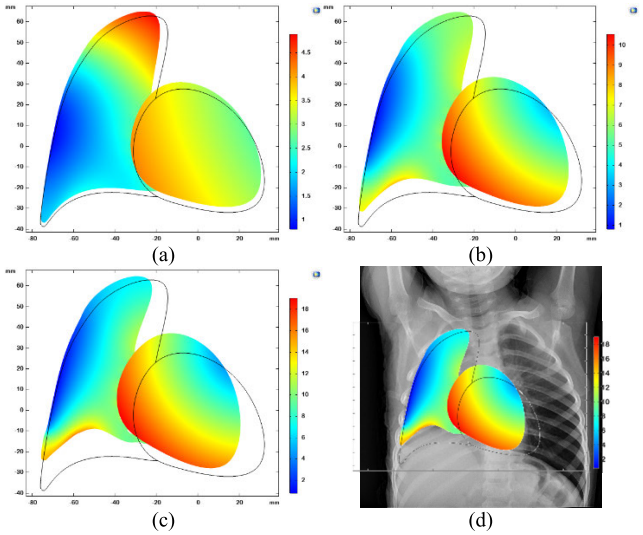

FIGURE 9. Total displacement at right lateral with (a) 10%, (b) 50%, (c) 100% of the total load, (d) superimposition of results on the corresponding X-ray image.

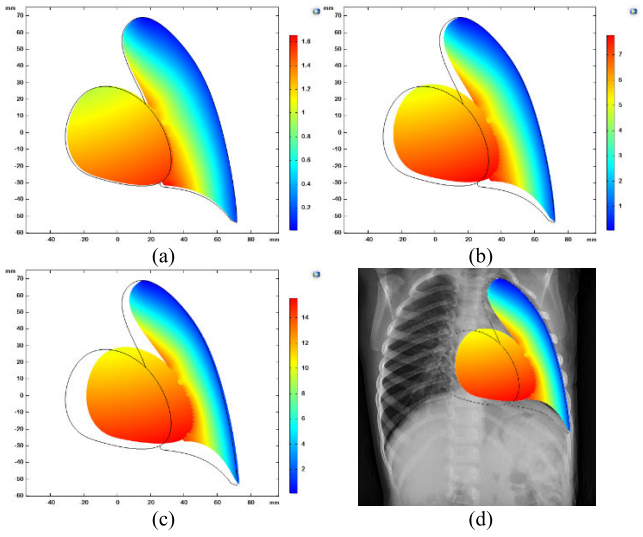

FIGURE 10. Total displacement at left lateral with (a) 10%, (b) 50%, (c) 100% of the total load, (d) superimposition of results on the corresponding X-ray image.

position followed by the situation where the recumbency dependent changes were accounted for, within the assumed model. Silent spaces were calculated in both schemes. Evidently if the calculated values would be relatively comparable then there would be no reason to consider the anatomical changes in the model/ROI; otherwise, one should incorporate this consideration when presenting the silent space values.

The CT scans of 10 patients within the age range of 1 to 2 years old including 5 males and 5 females, detailed in Table. 2 were used to design realistic 3D models. Parameter 'm' stands for male whereas the 'f' represents female with '*' indicating the data regarding that table cell was not available.

In lateral recumbency only the dependent lung is ventilated during tidal breathing thus the EIT signal for each patient was

TABLE 2. Patient specifications.

ID	Gender	Age (yrs)	Weight (g)
01	m	1.43	10200
02	f	1.07	*
03	m	1.68	12000
04	f	1.15	9735
05	m	1.52	8000
06	m	2.05	12000
07	f	1.86	*
08	m	1.09	10400
09	f	1.04	9785
10	f	1.19	7900

generated assuming altering air content only in the dependent lung. Since the CT scans were taken during the supine positions, the lateral situations had to be simulated. The required mechanical properties were set according to values verified earlier via X ray images.

To demonstrate the effect on EIT reconstructed images and consequently on silent spaces, two reconstruction algorithms were applied, namely, GREIT [34] and truncated Singular Value Decomposition (tSVD) [35]. In chest EIT the forward problem in charge of relating the unknown conductivity image to the measured boundary voltages is often assumed to be linear as the magnitude of conductivity change during breathing is bounded by the physiology, hence:

$$\mathbf{g} = \mathbf{A}\mathbf{x} \tag{4}$$

where $\mathbf{g}$ is the change in measured voltage differences on the electrodes attached to the surface and generated by injecting known currents to the domain, $\mathbf{x}$ stands for change in conductivity (image) and $\mathbf{A}$ presents sensitivity matrix containing the Jacobians $\mathbf{A}_{ij} = \frac{\partial \mathbf{y}_i}{\partial \mathbf{x}_j}$. Various algorithms exist based on the manner $\mathbf{A}$ is built and later inverted (reconstruction matrix) to achieve the desired image $\mathbf{x}$. The GREIT creates the reconstruction matrix via introducing a set of known training targets distributed at various positions in the domain and tries to form the reconstruction matrix $\mathbf{R}$ by minimizing the error norm between known image and the estimated one as:

$$\mathbf{R} = \arg min \left(\sum_{k=1}^{Number\ of\ trainings} \left\| \mathbf{x_k} - \hat{\mathbf{x}}_\mathbf{k} \right\|_{\mathrm{W}_k^2} \right) \tag{5}$$

where

$$\hat{\mathbf{x}}_\mathbf{k} = \mathbf{R}(\mathbf{g_k} + \mathbf{n}) \tag{6}$$

with $\mathbf{n}$ indicating the added noise on voltage data and the weights $\mathbf{W}_k$ offer the possibility of emphasizing on certain data sets/locations if needed, $\mathbf{R}$ is the reconstruction matrix and $\hat{\mathbf{x}}_k$ represents the estimated image from the k^{th} training data set.

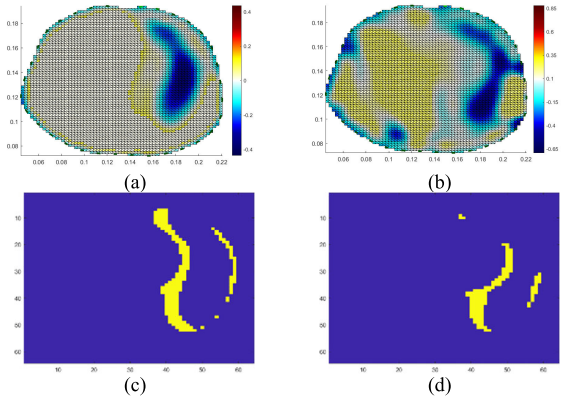

FIGURE 11. Using a common EIT signal, generated at left lateral mode and reconstructing images assuming a prior model and ROI via GREIT algorithm at (a) supine mode, (b) left lateral mode, the corresponding silent spaces at dependent left lung at (c) supine, (d) left lateral.

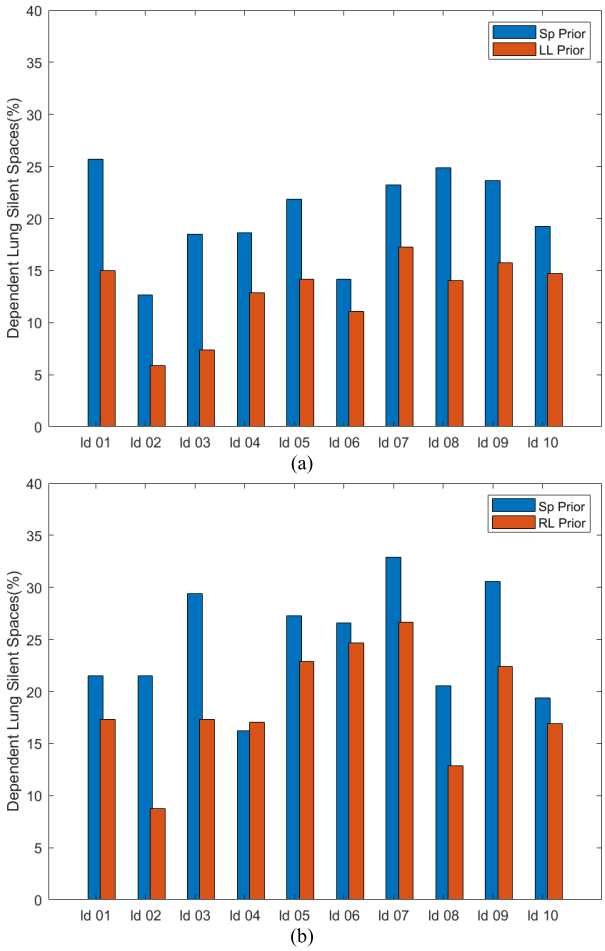

FIGURE 12. The dependent lung calculated silent spaces via GREIT algorithm with supine prior model in blue and right lateral prior in red for (a) left lateral, (b) right lateral modes.

The second algorithm applied, decomposes system matrix $\mathbf{A}$ as:

$$\mathbf{A} = \mathbf{U}\Sigma\mathbf{V}^{\mathbf{T}} \tag{7}$$

$$\mathbf{R} = \mathbf{A}^{\dagger} = \mathbf{V}\boldsymbol{\Sigma}^{-1}\mathbf{U}^{\mathbf{T}} \tag{8}$$

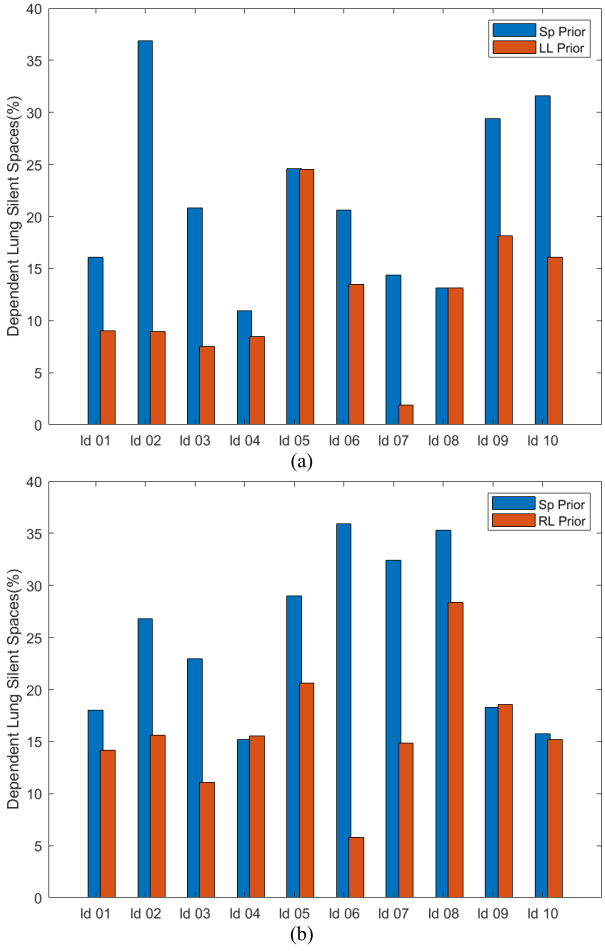

FIGURE 13. The dependent lung calculated silent spaces via tSVD algorithm with supine prior model in blue and right lateral prior in red for (a) left lateral, (b) right lateral modes.

where the singular values in the diagonal matrix $\boldsymbol{\Sigma}$ present how the basis vectors of $\mathbf{A}$ would affect the measured voltages when inverted. Therefore, the small singular values of $\mathbf{A}$ which carry little information yet can significantly amplify the noise during inversion are neglected and the reconstruction matrix is built upon the truncated matrix $\mathbf{A}$, keeping the first p number of singular values $\mathbf{s} = \{s_1, \ldots, s_p\}$ instead:

$$\mathbf{R}_p = \mathbf{V}_p\boldsymbol{\Sigma}_p^{-1}\mathbf{U}_p^{\mathbf{T}} \tag{9}$$

III. RESULTS

The simulated EIT signal was generated assuming 32 equally spaced electrodes with injection and measurement at skip 4 pattern at duration of 200 frames. Electrode potentials were further corrupted with 10% noise.

Here for GREIT algorithm the training was done via circular targets of size 0.1 (10% of maximum domain radius) and a noise figure of 0.5 implying the signal to noise ratio of image being half of the data whereas truncation threshold of 0.3 (i.e., $\frac{s_p}{s_1} = 0.3$) has been chosen for the tSVD method.

The background electric conductivity was assumed to be 1 Sm-1 with the dependent lung conductivity reduced

TABLE 3. Dependent lung silent space values based on using lateral and supine prior models.

ID	Patient at Right Lateral				Patient at Left Lateral			
	GREIT Reconstruction		tSVD Reconstruction		GREIT Reconstruction		tSVD Reconstruction	
	Prior Model Supine	Prior Model Right Lateral	Prior Model Supine	Prior Model Right Lateral	Prior Model Supine	Prior Model Left Lateral	Prior Model Supine	Prior Model Left Lateral
1	$\mu = 0.2152$ $\sigma = 0.0887$	$\mu = 0.1734$ $\sigma = 0.0643$	$\mu = 0.1798$ $\sigma = 0.0024$	$\mu = 0.1415$ $\sigma = 0.0017$	$\mu = 0.2569$ $\sigma = 0.0766$	$\mu = 0.1500$ $\sigma = 0.0826$	$\mu = 0.1608$ $\sigma = 0.0033$	$\mu = 0.0903$ $\sigma = 0.0029$
2	$\mu = 0.2152$ $\sigma = 0.1162$	$\mu = 0.0872$ $\sigma = 0.0591$	$\mu = 0.2678$ $\sigma = 0.0064$	$\mu = 0.1562$ $\sigma = 0.0016$	$\mu = 0.1264$ $\sigma = 0.0658$	$\mu = 0.0588$ $\sigma = 0.0689$	$\mu = 0.3685$ $\sigma = 0.0036$	$\mu = 0.0896$ $\sigma = 0.0032$
3	$\mu = 0.2940$ $\sigma = 0.0909$	$\mu = 0.1735$ $\sigma = 0.0763$	$\mu = 0.2297$ $\sigma = 0.0067$	$\mu = 0.1109$ $\sigma = 0.0029$	$\mu = 0.1847$ $\sigma = 0.0609$	$\mu = 0.0735$ $\sigma = 0.0573$	$\mu = 0.2081$ $\sigma = 0.0030$	$\mu = 0.0755$ $\sigma = 0.0012$
4	$\mu = 0.1622$ $\sigma = 0.0576$	$\mu = 0.1708$ $\sigma = 0.0694$	$\mu = 0.1519$ $\sigma = 0.0043$	$\mu = 0.1552$ $\sigma = 0.0035$	$\mu = 0.1861$ $\sigma = 0.0733$	$\mu = 0.1288$ $\sigma = 0.0673$	$\mu = 0.1095$ $\sigma = 0.0051$	$\mu = 0.0849$ $\sigma = 0.0036$
5	$\mu = 0.2730$ $\sigma = 0.0617$	$\mu = 0.2286$ $\sigma = 0.0573$	$\mu = 0.2896$ $\sigma = 0.0020$	$\mu = 0.2061$ $\sigma = 0.0024$	$\mu = 0.2189$ $\sigma = 0.0755$	$\mu = 0.1416$ $\sigma = 0.0662$	$\mu = 0.2457$ $\sigma = 0.0041$	$\mu = 0.2449$ $\sigma = 0.0030$
6	$\mu = 0.2656$ $\sigma = 0.0639$	$\mu = 0.2466$ $\sigma = 0.0756$	$\mu = 0.3591$ $\sigma = 0.0011$	$\mu = 0.0578$ $\sigma = 0.0013$	$\mu = 0.1415$ $\sigma = 0.0783$	$\mu = 0.1110$ $\sigma = 0.0769$	$\mu = 0.2058$ $\sigma = 0.0031$	$\mu = 0.1348$ $\sigma = 0.0040$
7	$\mu = 0.3288$ $\sigma = 0.0809$	$\mu = 0.2664$ $\sigma = 0.0751$	$\mu = 0.3243$ $\sigma = 0.0045$	$\mu = 0.1486$ $\sigma = 0.0053$	$\mu = 0.2325$ $\sigma = 0.0755$	$\mu = 0.1722$ $\sigma = 0.0778$	$\mu = 0.1435$ $\sigma = 0.0073$	$\mu = 0.0190$ $\sigma = 0.0018$
8	$\mu = 0.2056$ $\sigma = 0.0733$	$\mu = 0.1289$ $\sigma = 0.0436$	$\mu = 0.3531$ $\sigma = 0.0027$	$\mu = 0.2835$ $\sigma = 0.0075$	$\mu = 0.2486$ $\sigma = 0.0768$	$\mu = 0.1403$ $\sigma = 0.0553$	$\mu = 0.1311$ $\sigma = 0.0010$	$\mu = 0.1312$ $\sigma = 0.0028$
9	$\mu = 0.3055$ $\sigma = 0.0895$	$\mu = 0.2238$ $\sigma = 0.1021$	$\mu = 0.1832$ $\sigma = 0.0061$	$\mu = 0.1859$ $\sigma = 0.0056$	$\mu = 0.2361$ $\sigma = 0.0890$	$\mu = 0.1578$ $\sigma = 0.0658$	$\mu = 0.2939$ $\sigma = 0.0051$	$\mu = 0.1816$ $\sigma = 0.0068$
10	$\mu = 0.1942$ $\sigma = 0.0563$	$\mu = 0.1694$ $\sigma = 0.0566$	$\mu = 0.1578$ $\sigma = 0.0039$	$\mu = 0.1522$ $\sigma = 0.0012$	$\mu = 0.1925$ $\sigma = 0.0676$	$\mu = 0.1469$ $\sigma = 0.0602$	$\mu = 0.3160$ $\sigma = 0.0025$	$\mu = 0.1609$ $\sigma = 0.0015$

μ and σ stand for mean and standard deviation of the 200 iteration for calculating the silent spaces.

to 0.3 S.m-1 to represent relative air volume change. The assigned values and parameters were kept constant for all cases throughout the study.

An example when the EIT signal is generated at left lateral mode whereas images are reconstructed with assumptions at default supine versus recumbency consistent left lateral are plotted in Fig. 11(a) and Fig. 11(b) together with their corresponding left lung silent spaces in Fig.11(c) and Fig.11(d) at an arbitrary time frame for patient number 9 and applying the GREIT algorithm.

For each member from the 10 patients set under study, an EIT signal (as boundary voltages) was simulated assuming the patient in either left or right lateral position with the corresponding dependent lung being filled with air. Subsequent to additional noise, every generated signal was used to reconstruct images, once when the corresponding patient's default supine model/ROI was applied followed by the case where the recumbency consistent lateral counterparts were implemented.

As the dependent lung was assumed to be filled completely with air during EIT signal generation, in an ideal, noiseless situation one would expect the silent spaces to be zero.

The silent spaces were calculated for both scenarios and results are reported in bar chart format in Fig. 12 with GREIT as the reconstruction algorithm and in Fig. 13 while applying tSVD. The statistics regarding each case are written in Table 3.

The maximum improvements in case of tSVD were 27.8% and 30.1% in left and right laterals respectively whereas the same quantities reduced to 11.1% and 12.8% when GREIT was applied.

IV. DISCUSSION

It is evident from the results that the application of a model/ROI consistent with the patient recumbency position could improve the calculations of silent spaces, however, the amount of such improvements may vary. This is mainly due to genetical and pathological differences among patients meaning at under arm level where the EIT belt is often instructed to be placed, the internal organ contours corresponding to the planar cross section of the chest, differ from one patient to another. Therefore, the effect of movement of the heart and mediastinum as the consequence of change in patient recumbency position wouldn't stay identical thus making it infeasible to introduce a conclusive trend at least within a small statistical population.

One solution to this problem is using frontal chest X-ray images as a guide. This type of image is often available even at neonatal age range as they provide diagnostic information while the radiation dosage is significantly less than CT scanning. Such an image could point out at the desired height equal to under arm level hence how much the contours could potentially be affected by the internal movements. Evaluating the results obtained in this work, it seems the less heart cross section is involved in the contours the less the impact would be since the ratio of lungs cross section area to the area of mediastinum increases and results become less sensitive to the movements.

Fig. 14 demonstrates two examples to point out this issue related to patient Id 07 plotted on top panels and Id 04 on the bottom ones. Each row contains the chest cross-section at nipple line level at the left versus the frontal view on the right-hand side. It is evident that patient with Id 07 has more area

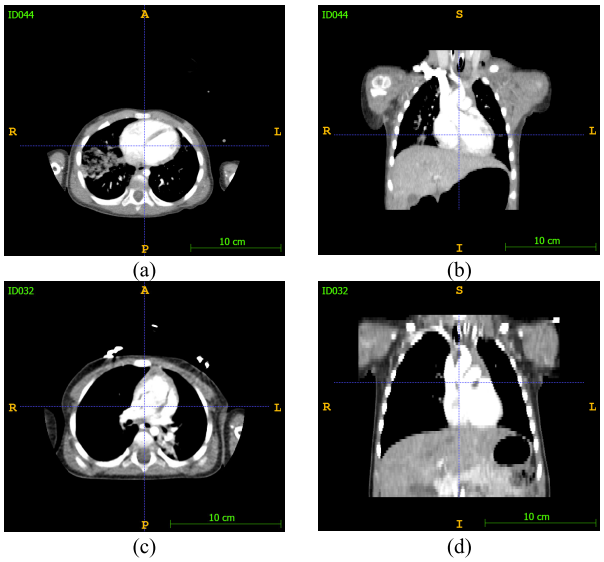

FIGURE 14. The CT scans of the patients at the nipple line level left panels and corresponding coronal images on the right panels of (a)-(b) Id 07, (c)-(d) Id 04.

occupied by the heart relative to the equivalent transversal slice shown for patient with Id 04. Therefore, following the recumbency position movements one should expect a higher impact on the calculated silent spaces for Id 07.

The other aspect is related to the calculated values with different reconstruction algorithms. As also shown earlier in [21] the GREIT algorithm smoothens the effect of prior model application via the optimization process implemented during formation of the reconstruction matrix. This would provide the flexibility for the algorithm to partly compensate for the application of improper prior model by adjusting weights within the training step. On the contrary as plotted in Fig. 13, tSVD reveals clearly the effect of the applied prior models. In addition, since in tSVD the small singular values are truncated the remaining independent columns in reconstruction matrix have little potential to amplify noise. Therefore, the standard deviations on the calculated results from a noisy signal are considerably lower relative to GREIT algorithm.

Finally, it should be noted in this work the outer shape of the chest is assumed to remain constant as the recumbency positions change which is not accurate and it is only done as it would facilitate identifying the impact of internal organ movements.

V. CONCLUSION

This study evaluated the internal organs movements within the thorax region and showed the possible impact of displacements/deformations that occur during recumbency position change on the silent spaces. The potential improvements amid applying a posture consistent model/ROI against the usage of their corresponding default mode as supine, are evident in both implemented reconstruction algorithms. The results presented here could also be useful, when an adequate estimation of model/ROI is not be available to provide an insight how the calculated silent spaces values change in relative terms as patient switch recumbency.

The results suggest that more cases are still required for reaching a conclusive verdict such as introducing a compensation factor according to recumbency position. For instance, when a patient is switched from supine to lateral the calculated silent spaces which would still be based on supine situation could be multiplied by this factor (less than one and depending on the contribution of heart portion in electrode 2D plane) as the dependent lung capacity would reduce amid the displacement/deformation of internal organs. Furthermore, a more comprehensive simulation should be conducted in 3D as the next step to include possible displacements/rotations in transversal and sagittal planes to evaluate their effect in changing the ROI during various recumbency modes as the performed simulations here are among the first ones in such category.

REFERENCES

[1] D. C. Barber and B. H. Brown, "Applied potential tomography," *J. Phys. E, Sci. Instrum.*, vol. 17, no. 9, pp. 723–733, Sep. 1984, doi: 10.1088/0022-3735/17/9/002.

[2] B. Rigaud, J.-P. Morucci, and N. Chauveau, "Bioelectrical impedance techniques in medicine. Part I: Bioimpedance measurement second section: Impedance spectrometry," *Crit. Rev. Biomed. Eng.*, vol. 24, nos. 4–6, pp. 257–351, 1996, doi: 10.1615/CritRevBiomedEng.v24.i4-6.20.

[3] Y. Shi, Y. Wu, M. Wang, Z. Tian, X. Kong, and X. He, "Sparse image reconstruction of intracerebral hemorrhage with electrical impedance tomography," *J. Med. Imag.*, vol. 8, no. 1, Jan. 2021, Art. no. 014501, doi: 10.1117/1.JMI.8.1.014501.

[4] A. Witkowska-Wrobel, K. Aristovich, M. Faulkner, J. Avery, and D. Holder, "Feasibility of imaging epileptic seizure onset with EIT and depth electrodes," *NeuroImage*, vol. 173, pp. 311–321, Jun. 2018, doi: 10.1016/J.NEUROIMAGE.2018.02.056.

[5] S. Hannan, M. Faulkner, K. Aristovich, J. Avery, M. C. Walker, and D. S. Holder, "In vivo imaging of deep neural activity from the cortical surface during hippocampal epileptiform events in the rat brain using electrical impedance tomography," *NeuroImage*, vol. 209, Apr. 2020, Art. no. 116525, doi: 10.1016/J.NEUROIMAGE.2020.116525.

[6] R. J. Halter, A. Hartov, S. P. Poplack, R. diFlorio-Alexander, W. A. Wells, K. M. Rosenkranz, R. J. Barth, P. A. Kaufman, and K. D. Paulsen, "Real-time electrical impedance variations in women with and without breast cancer," *IEEE Trans. Med. Imag.*, vol. 34, no. 1, pp. 38–48, Jan. 2015, doi: 10.1109/TMI.2014.2342719.

[7] S. Mansouri, T. Alhadidi, and M. B. Azouz, "Breast cancer detection using low-frequency bioimpedance device," *J. Breast Cancer*, vol. 12, pp. 109–116, Sep. 2020, doi: 10.2147/BCTT.S274421.

[8] D. Haemmerich, S. T. Staelin, J. Z. Tsai, S. Tungjitkusolmun, D. M. Mahvi, and J. G. Webster, "In vivo electrical conductivity of hepatic tumours," *Physiol. Meas.*, vol. 24, no. 2, pp. 251–260, May 2003, doi: 10.1088/0967-3334/24/2/302.

[9] Z. Zhao, F. Fu, and I. Frerichs, "Thoracic electrical impedance tomography in Chinese hospitals: A review of clinical research and daily applications," *Physiol. Meas.*, vol. 41, no. 4, Apr. 2020, Art. no. 04TR01, doi: 10.1088/1361-6579/ab81df.

[10] Z. Zhao, H. He, J. Luo, A. Adler, X. Zhang, R. Liu, Y. Lan, S. Lu, X. Luo, Y. Lei, I. Frerichs, X. Huang, and K. Möller, "Detection of pulmonary oedema by electrical impedance tomography: Validation of previously proposed approaches in a clinical setting," *Physiol. Meas.*, vol. 40, no. 5, 2019, Art. no. 054008, doi: 10.1088/1361-6579/AB1D90.

[11] S. J. H. Heines, U. Strauch, M. C. G. van de Poll, P. M. H. J. Roekaerts, and D. C. J. J. Bergmans, "Clinical implementation of electric impedance tomography in the treatment of ARDS: A single centre experience," *J. Clin. Monit. Comput.*, vol. 33, no. 2, pp. 291–300, Apr. 2019, doi: 10.1007/S10877-018-0164-X.

[12] T. H. Becher, M. Miedema, M. Kallio, T. Papadouri, C. Karaoli, L. Sophocleous, M. Rahtu, R. W. van Leuteren, A. D. Waldmann, C. Strodthoff, R. Yerworth, A. Dupré, M.-R. Benissa, S. Nordebo, D. Khodadad, R. Bayford, R. Vliegenthart, P. C. Rimensberger, A. H. van Kaam, and I. Frerichs, "Prolonged continuous monitoring of regional lung function in infants with respiratory failure," *Ann. Amer. Thoracic Soc.*, vol. 19, no. 6, pp. 991–999, Jun. 2022, doi: 10.1513/ANNALSATS.202005-562OC.

[13] M. Kallio, A.-S. van der Zwaag, A. D. Waldmann, M. Rahtu, M. Miedema, T. Papadouri, A. H. van Kaam, P. C. Rimensberger, R. Bayford, and I. Frerichs, "Initial observations on the effect of repeated surfactant dose on lung volume and ventilation in neonatal respiratory distress syndrome," *Neonatology*, vol. 116, no. 4, pp. 385–389, 2019, doi: 10.1159/000502612.

[14] A. Borsic, B. M. Graham, A. Adler, and W. R. B. Lionheart, "Total variation regularization in electrical impedance tomography," Manchester Inst. Math. Sci., Manchester, U.K., Tech. Rep. 1842, 2007.

[15] M. T. Clay and T. C. Ferree, "Weighted regularization in electrical impedance tomography with applications to acute cerebral stroke," *IEEE Trans. Med. Imag.*, vol. 21, no. 6, pp. 629–638, Jun. 2002, doi: 10.1109/TMI.2002.800572.

[16] M. Salucci, G. Oliveri, and A. Massa, "Real-time electrical impedance tomography of the human chest by means of a learning-by-examples method," *IEEE J. Electromagn., RF Microw. Med. Biol.*, vol. 3, no. 2, pp. 88–96, Jun. 2019, doi: 10.1109/JERM.2019.2893217.

[17] Z. Lin, R. Guo, K. Zhang, M. Li, F. Yang, S. Xu, D. Liu, and A. Abubakar, "Feature-based inversion using variational autoencoder for electrical impedance tomography," *IEEE Trans. Instrum. Meas.*, vol. 71, pp. 1–12, 2022, doi: 10.1109/TIM.2022.3192054.

[18] Z. Wei and X. Chen, "Induced-current learning method for nonlinear reconstructions in electrical impedance tomography," *IEEE Trans. Med. Imag.*, vol. 39, no. 5, pp. 1326–1334, May 2020, doi: 10.1109/TMI.2019.2948909.

[19] K. Zhang, M. Li, F. Yang, S. Xu, and A. Abubakar, "Three-dimensional electrical impedance tomography with multiplicative regularization," *IEEE Trans. Biomed. Eng.*, vol. 66, no. 9, pp. 2470–2480, Sep. 2019, doi: 10.1109/TBME.2018.2890410.

[20] J.-F.-P. J. Abascal, S. R. Arridge, D. Atkinson, R. Horesh, L. Fabrizi, M. De Lucia, L. Horesh, R. H. Bayford, and D. S. Holder, "Use of anisotropic modelling in electrical impedance tomography; description of method and preliminary assessment of utility in imaging brain function in the adult human head," *NeuroImage*, vol. 43, no. 2, pp. 258–268, Nov. 2008, doi: 10.1016/J.NEUROIMAGE.2008.07.023.

[21] N. Seifnaraghi, S. de Gelidi, S. Nordebo, M. Kallio, I. Frerichs, A. Tizzard, M. Suo-Palosaari, L. Sophocleous, A. H. van Kaam, E. Sorantin, A. Demosthenous, and R. H. Bayford, "Model selection based algorithm in neonatal chest EIT," *IEEE Trans. Biomed. Eng.*, vol. 68, no. 9, pp. 2752–2763, Sep. 2021, doi: 10.1109/TBME.2021.3053463.

[22] S. de Gelidi, N. Seifnaraghi, A. Bardill, A. Tizzard, Y. Wu, E. Sorantin, S. Nordebo, A. Demosthenous, and R. Bayford, "Torso shape detection to improve lung monitoring," *Physiol. Meas.*, vol. 39, no. 7, Jul. 2018, Art. no. 074001. [Online]. Available: http://stacks.iop.org/0967-3334/39/i=7/a=074001

[23] J. R. Lincoln and H. P. Sawyer, "Complications related to body positions during surgical procedures," *Anesthesiology*, vol. 22, no. 5, pp. 800–809, Sep. 1961, doi: 10.1097/00000542-196109000-00014.

[24] C. Klingstedt, G. Hedenstierna, H. Lundquist, A. Strandberg, L. Tgkics, and B. Brismar, "The influence of body position and differential ventilation on lung dimensions and atelectasis formation in anaesthetized man," *Acta Anaesthesiol. Scand.*, vol. 34, no. 4, pp. 315–322, May 1990, doi: 10.1111/J.1399-6576.1990.TB03094.X.

[25] A. D. Waldmann, P. L. Róka, S. Bohm, W. Windisch, S. Strassmann, and C. Karagiannidis, "Assessment of silent spaces at different PEEP levels by electrical impedance tomography in severe COPD," *Intensive Care Med. Exp.*, vol. 3, no. S1, p. A456, 2015, doi: 10.1186/2197-425X-3-S1-A456.

[26] I. Frerichs and T. Becher, "Chest electrical impedance tomography measures in neonatology and paediatrics—A survey on clinical usefulness," *Physiol. Meas.*, vol. 40, no. 5, Jun. 2019, Art. no. 054001, doi: 10.1088/1361-6579/ab1946.

[27] S. J. Lai-Fook, "Lung tissue mechanics," in *Respiratory Biomechanics*. New York, NY, USA: Springer, 1990, doi: 10.1007/978-1-4612-3452-4_4.

[28] A. Murphy, "Chest (lateral decubitus view)," Radiopaedia Australia Pty Ltd, Australia, Tech. Rep. 53650, May 2017. [Online]. Available: https://Radiopaedia.org, doi: 10.53347/RID-53650.

[29] V. P. Vellody, M. Nassery, W. S. Druz, and J. T. Sharp, "Effects of body position change on thoracoabdominal motion," *J. Appl. Physiol.*, vol. 45, no. 4, pp. 581–589, Oct. 1978, doi: 10.1152/JAPPL.1978.45.4.581.

[30] R. D. Adams and H. C. Pillsbury, "Position and activities of the diaphragm as affected by changes of posture," *Arch. Internal Med.*, vol. 29, no. 2, pp. 245–252, 1922, doi: 10.1001/ARCHINTE.1922.00110020104005.

[31] A. Kalra, C. J. Wehrle, and F. Tuma, *Anatomy, Abdomen and Pelvis, Peritoneum*. Tampa, FL, USA: StatPearls, Jul. 2021, Accessed: Jul. 15, 2022. [Online]. Available: https://www.ncbi.nlm.nih.gov/books/NBK534788/

[32] F. Polgar, "The action of gravity on the visceral cavity," *Acta Radiol.*, vol. 27, no. 6, pp. 647–665, Jan. 1946, doi: 10.3109/00016924609170121.

[33] A. Hostettler, D. George, Y. Rémond, S. A. Nicolau, L. Soler, and J. Marescaux, "Bulk modulus and volume variation measurement of the liver and the kidneys in vivo using abdominal kinetics during free breathing," *Comput. Methods Programs Biomed.*, vol. 100, no. 2, pp. 149–157, Nov. 2010, doi: 10.1016/J.CMPB.2010.03.003.

[34] A. S. Naini, R. V. Patel, and A. Samani, "Measurement of lung hyperelastic properties using inverse finite element approach," *IEEE Trans. Biomed. Eng.*, vol. 58, no. 10, pp. 2852–2859, Oct. 2011, doi: 10.1109/TBME.2011.2160637.

[35] R. De Wilde, J. Clement, J. M. Hellemans, M. Decramer, M. Demedts, R. Boving, and K. P. Van de Woestijne, "Model of elasticity of the human lung," *J. Appl. Physiol.*, vol. 51, no. 2, pp. 254–261, Aug. 1981, doi: 10.1152/JAPPL.1981.51.2.254.

[36] S. J. Lai-Fook and R. E. Hyatt, "Effects of age on elastic moduli of human lungs," *J. Appl. Physiol.*, vol. 89, no. 1, pp. 163–168, Jul. 2000, doi: 10.1152/JAPPL.2000.89.1.163.

[37] C. A. D'Angelis, J. J. Coalson, and R. M. Ryan, "Structure of the respiratory system: Lower respiratory tract," in *Pediatric Critical Care*. St. Louis, MO, USA: Mosby, 2011, pp. 490–498, doi: 10.1016/B978-0-323-07307-3.10036-9.

[38] P. Persson, S. Lundin, and O. Stenqvist, "Transpulmonary and pleural pressure in a respiratory system model with an elastic recoiling lung and an expanding chest wall," *Intensive Care Med. Exp.*, vol. 4, no. 1, pp. 1–14, Dec. 2016, doi: 10.1186/S40635-016-0103-4.

[39] Z. J. Schoppen, L. C. Balmert, S. White, R. Olson, P. Arunkumar, L. M. Dellefave-Castillo, M. J. Puckelwartz, A. L. George, E. M. McNally, and G. Webster, "Prevalence of abnormal heart weight after sudden death in people younger than 40 years of age," *J. Amer. Heart Assoc.*, vol. 9, no. 18, p. 15699, Sep. 2020, doi: 10.1161/JAHA.120.015699.

[40] W. R. Shankle, B. H. Landing, and J. Gregg, "Normal organ weights of infants and children: Graphs of values by age, with confidence intervals," *Pediatric Pathol.*, vol. 1, no. 4, pp. 399–408, 2009, doi: 10.3109/15513818309025871.

[41] P. M. Zeek, "Heart weight: I. The weight of the normal human heart," *Arch. Pathol.*, vol. 34, pp. 820–832, Jan. 1942.

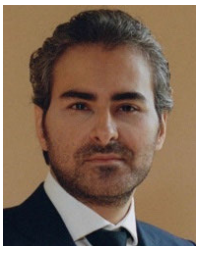

N. SEIFNARAGHI received the Ph.D. degree in electrical engineering from the Polytechnic University of Milan, in 2013. He has been a Research Fellow with the Polytechnic University of Milan and University College London. He is currently with Middlesex University London, U.K. His current research interests include biomedical engineering, applied mathematics, physics, modeling, and simulations.

S. DE GELIDI received the B.S. and M.S. degrees in biomedical engineering from the Polytechnic University of Milan and the Ph.D. degree in biomechanical engineering from the University of Portsmouth, in 2016.

She has been a Research Fellow with Middlesex University London, since 2016, where she was involved in the research and development of medical devices. Her current research interests include mechanical and electrical characterization, prototyping, and algorithm designs.

I. FRERICHS received the Ph.D. degree in physiology from Comenius University Bratislava, Slovakia (MD). She was with the Max Planck Institute for Experimental Medicine, Göttingen, Germany; Zürich University, Switzerland; and the University of Göttingen, Germany, for her research activities. Currently, she is a Professor of physiology with Christian-Albrechts University, Kiel, Germany. She is also the Head of the Electrical Impedance Tomography (EIT) Research Group, Department of Anaesthesiology and Intensive Care Medicine, University Medical Centre Schleswig-Holstein, Kiel Campus, Germany.

M. KALLIO received the degree in medicine from the University of Kuopio, in 2004, and the Ph.D. degree in medicine from the University of Oulu, in 2014. She was granted the title Docent of pediatric cardiology from the University of Oulu, in 2021. She is currently a Consultant Pediatric Cardiologist with the Helsinki New Children's Hospital and a Clinical Researcher with the PEDEGO Research Unit, University of Oulu, and the Oulu University Hospital, Finland. Her current research interest includes improving the quality of pediatric ventilation and intensive care.

MD. E. SORANTIN was born in 1957. He received the degree in medicine from the University of Vienna, in 1982, and the Ph.D. degree (Hons.) in informatics from the Faculty of Science, University of Szeged, Hungary, in 2018.

He worked in several hospitals, fulfilled training as a general practitioner, and became qualified as a pediatrician and a radiologist. In 1988, he joined the Team of the Department of Radiology, Medical University Graz, where he was a Faculty Member, in 1994, and earned his professorship, in 2002. Currently, he is the acting Head of the Division of Pediatric Radiology, Medical University Graz. Moreover, he coordinates a multi-institutional, multidisciplinary academic network in Central Europe, which focuses on biomedical imaging and technology transfer of advanced pediatric care and radiation protection. Additionally, he served as a Consultant of computer graphics for the medical vendor Siemens concentrating on virtual endoscopic techniques, for approximately eight years. During this cooperation, two products were brought to the market: the Virtuoso3D and the Leonardo Workstation. He was decorated with several awards.

A. DEMOSTHENOUS (Fellow, IEEE) received the B.Eng. degree in electrical and electronic engineering from the University of Leicester, Leicester, U.K., in 1992, the M.Sc. degree in telecommunications technology from Aston University, Birmingham, U.K., in 1994, and the Ph.D. degree in electronic and electrical engineering from University College London (UCL), London, U.K., in 1998. He is currently a Professor with the Department of Electronic and Electrical Engineering, UCL, and also leads the Analog and Biomedical Electronics Group. He has made outstanding contributions to improving safety and performance in integrated circuit design for active medical devices, such as spinal cord and brain stimulators. He has numerous collaborations for cross-disciplinary research, both within the U.K., and internationally. He has authored more than 350 papers in journals and international conference proceedings, several book chapters, and holds several patents. His current research interests include analog and mixed-signal integrated circuits for biomedical, sensor, and signal processing applications. He is a fellow of the Institution of Engineering and Technology and a Chartered Engineer. He was an Associate Editor and the Deputy Editor-in-Chief of the IEEE TRANSACTIONS ON CIRCUITS AND SYSTEMS—II: EXPRESS BRIEFS, from 2006 to 2007 and from 2014 to 2015, respectively, and an Associate Editor and the Editor-in-Chief of the IEEE TRANSACTIONS ON CIRCUITS AND SYSTEMS—I: REGULAR PAPERS, from 2008 to 2009 and from 2016 to 2019, respectively. He is an Associate Editor of the IEEE TRANSACTIONS ON BIOMEDICAL CIRCUITS AND SYSTEMS and serves on the International Advisory Board of *Physiological Measurement*. He has served on the technical committees for several international conferences.

R. H. BAYFORD (Life Senior Member, IEEE) received the M.Sc. degree in industrial systems from Cranfield University, Cranfield, U.K., and the Ph.D. degree from Middlesex University, London, U.K., in 1994.

He was a Professor of bio-modeling and informatics with the Department of Natural Sciences, Middlesex University London, U.K., in 2005. He is currently a Visiting Professor with the Department of Electrical and Electronic Engineering, University College London, London, U.K. He has authored more than 350 papers in journals and international conference proceedings and holds several patents. His current research interests include biomedical image/signal processing, electrical impedance tomography, deep brain stimulation, bio-modeling, telemedical systems, and VLSI designs.

Mr. Bayford is a fellow of the Institute of Physics. His awards and honors include the Frew Fellowship (Australian Academy of Science), the I. I. Rabi Prize (APS), the European Frequency and Time Forum Award, the Carl Zeiss Research Award, the William F. Meggers Award, and the Adolph Lomb Medal (OSA). He was the Editor-in-Chief of *Physiological Measurement* (Institute of Physics), from 2008 to 2013. He is on the editorial board of the *International Journal of Biomedical Imaging*.